Thermal Frequency Response Method for the Study of Mass-Transfer Kinetics in Adsorbents

V. Bourdin, Ph. Grenier, F. Meunier, and L. M. Sun
Limsi BP 133 F91403 Orsay, France

The frequency response method measuring the temperature and pressure of an adsorbent sample determines the mass- and heat-transfer kinetics in adsorbents, especially in zeolites. The temperature of the sample (large crystals or monolayers of pellets) is measured by infrared detection. The main aspects of the in-phase and out-of-phase functions as given by an analytical bidispersed model are described. They depend on characteristic times related to kinetic parameters. Experimental results on adsorption of water on NaX zeolite (crystals or pellets) show that this method allows heat transfer to be very clearly delineated from mass-transfer modes and the separation of different mass-transfer modes. For a bidispersed sample, macro- and microporous mass-transfer parameters may be obtained with the same sample. Results on a contaminated 5A zeolite-propane system show the presence of mass-transfer resistance at the pellet surface. The infrared temperature measurement associated with the frequency response appears to be powerful in determining kinetic adsorption, and gives more information than the pressure measurement.

Introduction

The frequency response (FR) method in kinetic studies, which consists of sinusoidal modulation of the volume of an experimental chamber and recording of the pressure, was first developed in the 1960s (Polinski and Naphtali, 1963) and 1970s (Evnochides and Hĕnley, 1970; Bétemps et al., 1977). It has attracted more attention in recent years to determine the mass-transfer kinetics in adsorbents (Van-Den-Begin and Rees, 1989; Jordi and Do, 1992; Yasuda, 1994; Sun et al., 1994). This development is due to the following advantages.

- The method transforms a transient system to a quasi-stationary one, allowing precise measurements that are insensitive to small changes in experimental conditions (e.g., drifts).
- The phase lag between pressure and volume is directly related to the characteristic times of the heat and mass transfer.
- The response is sensitive to the nature of the mass transfer: diffusion or surface barrier.

Nevertheless, it is difficult to account for the thermal effects when only the pressure is measured. The thermal effects always occur during adsorption; they affect the response and may lead to misinterpretations, if ignored (Sun et al., 1993; Sun and Bourdin, 1993).

Here we will describe a new method that consists of measuring the temperature of an adsorbent sample that has been submitted to volume modulation, as well as the pressure in the chamber, and then comparing the experimental and theoretical results.

General Considerations

The measurement of the temperature presents some unique aspects.

- The thermal effects are naturally taken into account.
- The amplitude of the sample temperature increases when the mass of the sample decreases and tends toward a limit that depends on the volume modulation rate and on the thermodynamic parameters of the adsorbent-adsorbate system. Thus, it is possible to work with a very small sample (for instance, a quasi monolayer of few micron crystals) and thus avoid spurious effects that occur when the bed is thick (Zhong et al., 1993).
- Pressure response is observed to be even when the chamber is empty and the sample acts only as a perturbation

Correspondence concerning this article should be addressed to Ph. Grenier.

of this response, while temperature response is intrinsic and obtained only when adsorption occurs. For high enough frequencies, the thermal relaxation is very small and the temperature response is directly proportional to the loading variation.

- When measured by infrared (IR) emission, the temperature is the surface temperature of the sample. This gives information about the thermal diffusivity of the sample that is not obtained by the pressure response.

Theoretical Studies

Let us consider an adsorbent sample placed in a chamber whose volume, V, varies periodically at angular frequency ω ($\omega = 2\pi f$) with an amplitude v independent of ω:

$$V = V_e(1 - ve^{i\omega t}). \tag{1}$$

where e denotes the mean value of the parameter. After a transient state, the pressure and the temperature become periodical functions of the time at the same frequency.

For the temperature

$$T = T_e + A_T(\omega)e^{i[\omega t + \varphi(\omega)]}, \tag{2}$$

which may also be written

$$\Delta T/\Delta V = \frac{A_T(\omega)}{v}e^{i\varphi(\omega)}, \tag{3}$$

where $\Delta V = V_e - V/V_e$, $\Delta T = T - T_e$ is the temperature variation around the constant temperature of the wall and $A_T(\omega)$ is the amplitude of the temperature variation. Because the relative volume amplitude v is small ($v \sim 0.02$), the system may be linearized, and $A_T(\omega)$ is proportional to v. The complex ratio $\theta = \Delta T/\Delta V$ expresses the time-dependent temperature, taking the volume as reference. It is independent of the time, and the system is quasistationary.

The pressure may be expressed as

$$P = P_e[1 + p(\omega)e^{i[\omega t + \psi(\omega)]}] \tag{4}$$

or

$$\Delta P/\Delta V = \frac{p(\omega)}{v}e^{i\psi(\omega)}, \tag{5}$$

where $\Delta P = P - P_e$ is the pressure variation around its mean value. The ratio $\Delta P/\Delta V$ is independent of the time, as is $\Delta T/\Delta V$. The phases of the temperature and pressure variations are noted as $\varphi(\omega)$ and $\psi(\omega)$, respectively. The complex functions $\Delta T/\Delta V$ and $\Delta P/\Delta V$ depend on the thermodynamic and kinetic properties of the sample. The most useful functions to identify the kinetic parameters from experimental data are, for the pressure (Yasuda, 1976):

$$\delta = \Delta V/\Delta P - 1, \tag{6}$$

which becomes in the real domain

$$\delta_{in} = \frac{v}{p}\cos\psi - 1 \qquad \delta_{out} = \frac{v}{p}\sin\psi, \tag{7}$$

which are the in-phase and out-of-phase functions, respectively.

For the temperature, these functions are (Sun et al., 1993):

$$\theta^v_{in} = A_T\cos\varphi \qquad \theta^v_{out} = A_T\sin\varphi. \tag{8}$$

Physically, the sample temperature variation is due to the thermal effect associated with the change of the adsorbed amount, which depends on the pressure. The pressure variation is induced by the volume variation and is theoretically only a function of the absorptive properties of the sample. However, the pressure change can be altered by spurious factors such as adsorption of the chamber walls and heating of the gas by nonisothermal compression. Thus, it is often advisable to express the temperature as a function of the pressure. Equations 3 and 5 lead to the following expression:

$$\Delta T/\Delta P = \frac{A_T}{p}e^{i(\varphi - \psi)}. \tag{9}$$

The corresponding real functions, which describe the complex function ΔT, are

$$\theta^p_{in} = \frac{v}{p}A_T\cos(\varphi - \psi) \qquad \theta^p_{out} = \frac{v}{p}A_T\sin(\varphi - \psi). \tag{10}$$

These functions are obtained by processing the experimental temperature data and taking the experimental pressure data as a reference. They are very useful since they describe the intrinsic behavior of the sample, independently of all parasitic effects.

Model

The model used to evaluate the functions p, A_T, φ, and ψ considers two scales of porosity for pellets and a single porosity for crystals. In the case of pellets that are all considered in the same physical condition, the gas first penetrates through the macropores (in some instances a film resistance may exist at the pellet surface). As the gas proceeds in the macropores, it reaches the crystals and has the opportunity to penetrate through the micropores. In some cases a barrier at the crystal surface must be passed through before the gas diffuses in the micropores. No assumption is made about the physical origin of such a surface barrier (or film resistance at macroporous scale), but it is assumed that a pressure drop proportional to the mass flux exists at the surface of the particle. It is introduced because, in many cases, pure Fickian diffusion is unable to explain the experimental results. The pellets as well as the crystals are assumed to be uniform in size (if desired, a size distribution may be included in the model) and of regular geometrical shape.

The heat released by sorption in the micropores has to be dissipated first through heat conduction in the pellet; then a heat exchange, described by an overall heat-transfer coefficient h including convective and radiative exchanges, proceeds toward the surrounding. The volume change induces a change in the gas temperature, because of the finite value of the heat exchange between the gas and the wall. The first consequence is an increase in the pressure amplitude com-

pared to the pressure amplitude in the isothermal case; the second consequence is a transfer of heat from the gas to the sample, leading to a slight change of its temperature. Nevertheless, the gas thermal relaxation on the wall is fast, and this last effect is almost negligible, especially at low frequency ($f < \sim 1$ Hz) (see hereafter the results on blank experiments). More details on these effects will be given in a subsequent article (Bourdin et al., 1996). For simplicity, the model presented here assumes that the gas temperature is constant and equal to T_e.

The volume change causes a pressure variation in the gas phase leading to adsorption–desorption in the adsorbent. Because of the small variation in volume, the adsorption isotherm may be linearized.

The mathematical treatment corresponding to these assumptions has been described (Sun et al., 1993). For a monodispersed sample (crystals), the equations of heat and mass transfer may be written as follows:

Overall Mass Balance

$$\frac{d}{dt}\left(\frac{PV}{R_eT}+V_s\bar{q}\right)=0, \tag{11}$$

where V_s is the sample volume, $\bar{q}$ is the average concentration of the sorbate volume, and R is the gas constant.

Mass Balance in the Crystal

$$\frac{\partial q}{\partial t}=\frac{D_c}{r_c^{\sigma}}\frac{\partial}{\partial r_c}\left(r_c^{\sigma}\frac{\partial q}{\partial r_c}\right), \quad -D_c\frac{\partial q}{\partial r}\bigg|_{r_c=R_c}=k_c(q|_{r_c=R_c}-q^*),$$

$$\frac{\partial q}{\partial r_c}\bigg|_{r_c=0}=0, \tag{12}$$

where σ is a shape factor ($\sigma = 0$, 1, or 2 for sheet, cylinder, or sphere, respectively), D_c is the microporous diffusion coefficient, and k_c is the surface barrier coefficient. The amount adsorbed at equilibrium q^* is given by

$$q^*-q_e=K_p(P-P_e)-K_T(T-T_e), \tag{13}$$

where q_e is the concentration at thermodynamical equilibrium for $P=P_e$ and $T=T_e$.

Energy Balance in the Crystal

$$C_s\frac{dT}{dt}+\frac{(\sigma+1)h}{R_c}(T-T_e)=|\Delta H|\frac{d\bar{q}}{dt}. \tag{14}$$

The temperature inside the crystals is considered to be uniform because the characteristic time of heat diffusion, even in the largest crystals (100-μm edge), is always less than 1 ms.

For bidispersed sample the equations become:

Overall Mass Balance

$$\frac{dc_g}{dt}+\frac{V_s}{V_e}\frac{d}{dt}\left[\epsilon\overline{c_p}+(1-\epsilon)\bar{q}\right]=0, \tag{15}$$

where ϵ is the porosity of the pellet.

Mass Balance in the Pellet

$$\frac{\partial c_p}{\partial t}+\frac{1-\epsilon}{\epsilon}\frac{\partial\bar{q}}{\partial t}=\frac{D_p}{r_p^{\nu}}\frac{\partial}{\partial r_p}\left(r_p^{\nu}\frac{\partial c_p}{\partial r_p}\right),$$

$$-D_p\frac{\partial c_p}{\partial r_p}\bigg|_{r_p=R_p}=k_p(c_p|_{r_p=R_p}-c_g),$$

$$\frac{\partial c_p}{\partial r_p}\bigg|_{r_p=0}=0, \tag{16}$$

where ν is the shape factor of the pellets ($\nu = 0$, 1, or 2 for sheet, cylinder, or sphere, respectively), D_p and k_p are the macropore mass-transfer coefficients, and c_p and c_g are the concentration in the gas phase inside the macropores and outside the pellet, respectively.

The resistance to heat diffusion in the pellet cannot be neglected, and the heat balance may be written as follows:

$$C_s\frac{\partial T}{\partial t}+(1-\epsilon)|\Delta H|\frac{\partial\bar{q}}{\partial t}=\frac{\lambda}{r_p^{\nu}}\frac{\partial}{\partial r_p}\left(r_p^{\nu}\frac{\partial T}{\partial r_p}\right),$$

$$-\lambda\frac{\partial T}{\partial r_p}\bigg|_{r_p=R_p}=h(T|_{r_p=R_p}-T_e), \quad \frac{\partial T}{\partial r_p}\bigg|_{r_p=0}=0. \tag{17}$$

The mathematical formulation that describes the surface barriers at the crystal and pellet surfaces gives no definite indication of the physical process involved. This process may be either an external effect, like pressure drop in the chamber, or an internal effect, like a change in the particle's mass diffusivity near the surface. The surface barrier coefficients k_p and k_s are introduced because, in many cases, experimental data cannot be adapted properly with Fickian diffusion alone.

The mathematical treatment allows the calculation of the pressure functions δ_{in} and δ_{out}, and the in-phase and out-of-phase temperature functions and $\theta_{in}^{\upsilon,p}/\theta_{out}^{\upsilon,p}$.

In the adiabatic case with instantaneous mass-transfer kinetics, $\theta_{in}^{\upsilon}=0$ and θ_{in}^{p} has the constant value A_M:

$$A_M^V=\frac{\upsilon\gamma\Lambda T_e}{(1+K+\gamma)}, \quad A_M^p=\frac{\upsilon\gamma\Lambda T_e}{(1+\gamma)} \tag{18}$$

where $\Lambda = K_p/K_TT_e$ and γ is a coefficient that describes the nonisothermality of the system. Its expression is

$$\gamma=\frac{|\Delta H|K_T}{C_s} \quad \text{or} \quad \gamma=\frac{(1-\epsilon)|\Delta H|}{C_s}K_T(1-\Lambda) \tag{19}$$

for crystals and pellets, respectively.

The normalized representation of the in-phase and out-of-phase functions is obtained by dividing the amplitude A_T by A_M^{υ} in the case of volume reference treatment, and dividing A_T by A_M^p in the case of pressure reference treatment. The corresponding normalized functions will be noted $\hat{\theta}^{\upsilon}$ and $\hat{\theta}^{p}$, respectively. For the pressure response, the normalized representation is obtained by dividing the characteristic functions by the adsorptive capacity coefficient K ($K =$

$R_eT_eK_pV_s/V_e$), which is the ratio of the variation of the adsorbed mass over the variation of the mass contained in the chamber for a given variation of the pressure. It will be noted $\hat{\delta}$.

We now examine the main features of the temperature response compared with the pressure response. First let us remark that the adsorbed amount and thus the pressure response amplitude both decrease due to thermal effects and to mass-transfer resistances. As a result, its maximum occurs at low frequency and it decreases when frequency increases. The out-of-phase function may present one or two maxima, depending on thermal and mass-transfer effects, and it may be rather difficult to distinguish between these two effects (Sun and Bourdin, 1993).

The thermal response is quite different: it is small at low frequency because the thermal relaxation is completed after a short period. As the frequency increases, a thermal response appears, and in the case of equilibrium adsorption, tends toward the limit A_M^v. But in the case of finite mass-transfer kinetics, the response falls at a frequency that depends on the mass-transfer characteristic time. The out-of-phase function presents a maximum at low frequency that corresponds to the heat-transfer limitations, and a minimum at high frequency that corresponds to the mass-transfer limitations. The thermal effect always corresponds to an increase in the temperature amplitude, and the mass-transfer limitation corresponds to a decrease in the temperature amplitude: the two transfer modes are thus much more clearly separated than in the case of the pressure response. Moreover, the domain covered by the phase lag is large, starting from $+\pi/2$ at low frequency, and reaching values between $-\pi/4$ and $-\pi/2$ at high frequency. In the case of the pressure response, the domain covered by the phase lag is always less than $\backsim \pi/4$.

Characteristic Times. Each special feature appearing in the characteristic function at an angular frequency ω (for instance, an extremum of the out-of-phase function) corresponds to a characteristic time t given by $\omega t \backsim 1$. These characteristic times depend on the mass-transfer kinetic parameters D_c, D_p, k_c, and k_p and on the heat-transfer parameters h and λ. Moreover, they depend on the adsorptive capacity coefficient K (a larger K corresponding to a faster kinetics). Thus, each kinetic parameter corresponds to a window in the frequency domain in which this parameter affects the shape of the characteristic functions, and this influence is different depending on the nature of the parameter. Thus, it is quite easy to identify these parameters separately.

The most useful characteristic times to describe the shape of the characteristic functions are those that appear in the ratio of the two first temperature moments during a pressure step (Torresan and Grenier, 1992). They depend only on the physical properties of the sample, and are independent of the coefficient K. Thus, the frequency windows corresponding to these times agree well with the main features of the characteristic functions θ_{in} and θ_{out} when the value of the K coefficient is not too large. These characteristic times are expressed as follows:

Microporous Mass Transfer

$$\tau_{Dc} = \frac{R_c^2}{(\sigma+1)(\sigma+3)D_c} \qquad \tau_{sc} = \frac{R_c}{(\sigma+1)k_c}. \tag{20}$$

Macroporous Mass Transfer

$$\tau_{D_p} = \frac{(1+\beta)R_p^2}{(\nu+1)(\nu+3)D_p}, \quad \tau_{sp} = \frac{(1+\beta)R_p}{(\nu+1)k_p}. \tag{21}$$

These times are the mean times of isothermal mass transfer after a pressure step.

Heat Transfer

$$\tau_h = \frac{[1+(1+\alpha)\gamma]C_sR_p}{(\nu+1)h}, \quad \tau_\lambda = \frac{[1+(1+\alpha)\gamma]C_sR_p^2}{(\nu+1)(\nu+3)\lambda}, \tag{22}$$

where τ_h is the thermal relaxation time of the sample with the surroundings, and τ_λ is the mean time of heat diffusion through a pellet after a temperature step. The parameters α and β are expressed as follows:

$$\alpha = \epsilon\frac{V_s}{V_e}, \qquad \beta = \frac{(1-\epsilon)}{\epsilon}R_eT_eK_p. \tag{23}$$

As pointed out previously, the characteristics of the temperature response depend on the relative values of the characteristic times. Typical results obtained by the model are presented to demonstrate the influence of the various characteristic times. The relevant parameters chosen to describe the typical cases are summarized Table 1, and the thermodynamic parameters used to run the model are close to those of the 5A-propane system.

1. The characteristic microporous diffusion time is much smaller than the heat transfer time: $\tau_h \gg \tau_{Dc}$ (monodispersed case, surface barrier neglected). This is the most com-

Table 1. Kinetic Parameters Introduced in the Model and Corresponding Characteristic Times for Typical Configurations

Figure	τ_{Dc} s	τ_{sc} s	τ_{Dp} s	τ_{sp} s	τ_h s	τ_λ s
1						
——	1				1,000	
- - -	1	0	0	0	500	0
------	2				1,000	
2						
——						3.6
------	0.1	0	10	0	1,000	0.9
- - -						0
3						
——	0.1	0	10	0	1,000	0.9
------	0.3					
4	0.01	0	25	0	1,000	0.5
5						
------	10				5	
- - -	5	0	0	0	10	0
——	10				10	
6						
——	10	0	0	0	500	0
------	0	10				

The values of the other parameters used to run the model are: $C_s = 1.4 \times 10^6$ J·kg^{-1}·K^{-1}; $|\Delta H| = 1.5\ 10^6$ J·kg^{-1}; $K_p = 0.019$ kg·m^{-3}·Pa^{-1}; $K_T = 1.54$ kg·m^{-3}·K^{-1}; $P_e = 900$ Pa; $T_e = 297$ K; $V_e = 6 \times 10^{-4}$ m^3; $V_s = 1.7 \times 10^{-6}$ m^3; $\epsilon = 0.4$, which give $\gamma \sim 1$ and $K = 2.8$.

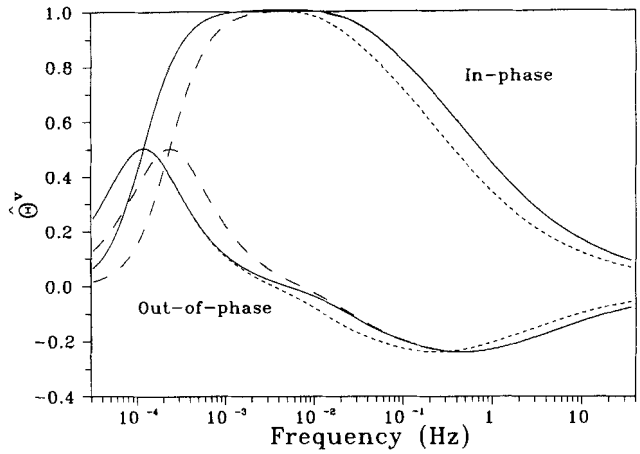

Figure 1. Calculated temperature characteristic functions $\hat{\theta}_{in}^{v}$ and $\hat{\theta}_{out}^{v}$ for (——) $\tau_h = 1{,}000$ s, $\tau_{Dc} = 1$ s; (------) $\tau_h = 1{,}000$ s, $\tau_{Dc} = 2$ s; (---) $\tau_h = 500$ s, $\tau_{Dc} = 1$ s.

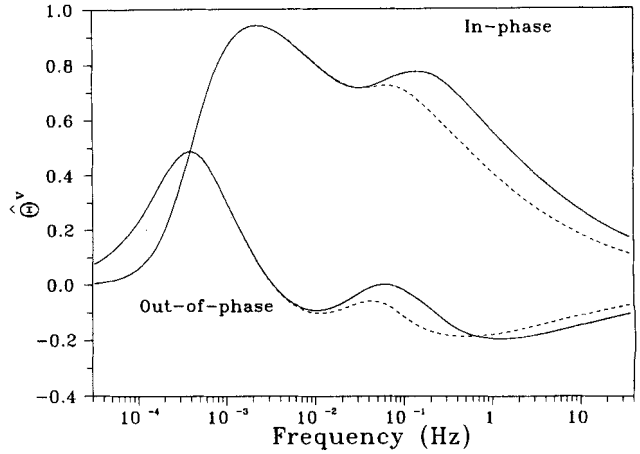

Figure 3. Calculated characteristic functions $\hat{\theta}_{in}^{v}$ and $\hat{\theta}_{out}^{v}$ for (---) $\tau_{Dc} = 0.3$ s; (——) $\tau_{Dc} = 0.1$ s.

mon case. Figure 1 shows that, in this case, only the low-frequency part of the characteristic functions is modified when τ_h is modified. On the other hand, only the high-frequency part is modified when τ_{Dc} is modified: that means that the heat- and the mass-transfer parameters affect different frequency ranges and, being uncoupled, may be identified separately.

2. The heat diffusion characteristic time in the pellet is not negligible. Figure 2 shows that the phase functions vary with the conductivity of the pellet, especially at high frequency (the characteristic time of heat diffusion in a pellet is of the order of 1 s). This allows us to identify the pellet conductivity, as is also possible with the volume step method (Grenier et al., 1995).

3. The microporous diffusion is much faster than the macroporous one. That is often the case because the pellets are made of small crystals, so diffusion characteristic time is very small. As a result of the finite conductivity of the pellet, the surface temperature measured by infrared detection does not depend on the macroporous mass-transfer diffusivity at high frequency, but only on the microporous mass transfer. This important effect occurs when the characteristic time of the heat diffusion in the pellet is smaller than the macroporous mass-transfer characteristic time and greater than the microporous one ($t_{Dp}/t_\lambda \gg 1$ and $(t_{Dc} + t_{sc})/t_\lambda \ll 1$, assuming the film resistance at the surface of the pellet is negligible). Because both τ_{Dp} and τ_λ depend on R_p^2, the first condition does not depend on the size of the pellet, and the condition $t_{Dp}/t_\lambda \gg 1$ is usually satisfied. The second condition is satisfied for high enough values of R_p. Figure 3 shows this effect, which allows us to determine both macro- and microporous mass-transfer kinetics with the same sample.

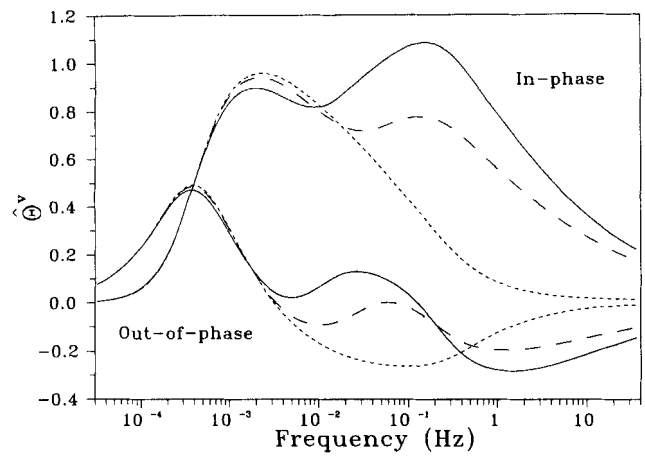

Figure 2. Calculated characteristic functions $\hat{\theta}_{in}^{v}$ and $\hat{\theta}_{out}^{v}$ for (——) $\tau_\lambda = 3.6$ s ($\lambda = 0.05$ W·m^{-1}·K^{-1}); (---) $\tau_\lambda = 0.9$ s ($\lambda = 0.2$ W·m^{-1}·K^{-1}); (------) $\tau_\lambda = 0$.

4. Case when $t_h > t_{Dp} > t_\lambda > t_{Dc}$ (surface barrier effects not taken into account). In this case, which is the most common, the four limiting effects are uncoupled as shown on Figure 4. The heat-transfer coefficient h affects only the lower frequency range and the macroporous diffusion coefficient affects the middle-frequency range. The thermal conductivity of the pellet and the microporous diffusion coefficient affect the high-frequency domain, but differently: for instantaneous microporous diffusion the in-phase function tends toward a nonzero limit whose value depends on the thermal conductivity. This function tends toward 0 at high frequency for a finite value of the microporous diffusivity. Figure 4a shows the characteristic functions for this important case. The maximum in the out-of-phase function corresponds to the thermal relaxation, the first minimum corresponds to the macroporous diffusion, and the second minimum corresponds to the microporous diffusion.

The possibility of determining the pellet conductivity and both the macro- and microporous mass-transfer kinetics with the same sample is specific to the infrared (IR) detection temperature response, especially with the frequency response technique: the pressure response always depends on the adsorbed mass averaged on the whole pellet, and is practically insensitive to the pellet conductivity and to the microporous diffusion when the macroporous diffusion is rate limiting, as shown on Figure 4b.

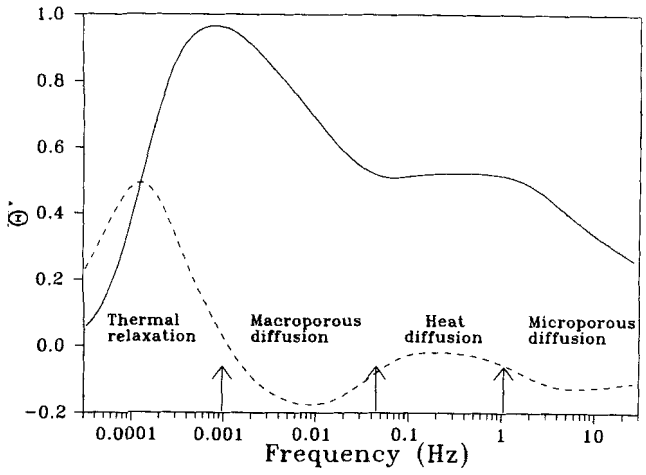

(a)

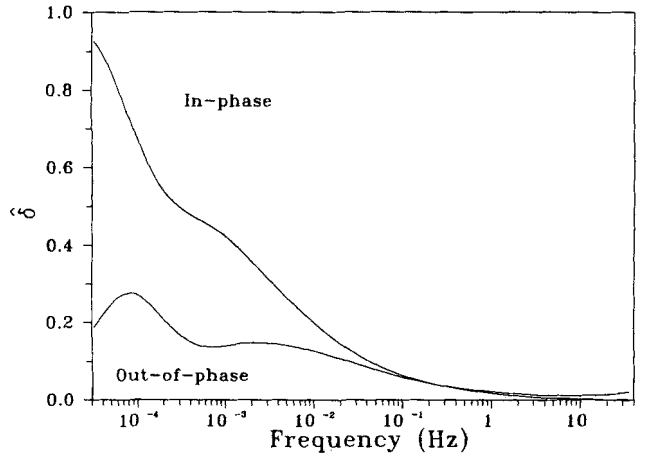

(b)

Figure 4. (a) Calculated $\hat{\theta}_{in}^{v}$ and $\hat{\theta}_{out}^{v}$ for $\tau_h = 1{,}000$ s; $\tau_{Dp} = 25$ s, $\tau_\lambda = 0.5$ s, and $\tau_{Dc} = 0.01$ s; (b) calculated pressure functions for the same parameters as for Figure 4a.

5. In the case when $\tau_h < \tau_{Dc}$ (quasi-isothermal case), the temperature response does not reach the maximum value A_M, and the position of the out-of-phase minimum is less sensitive to the mass-transfer characteristic time than in case 1 (Figure 5). Obviously, the method is not well adapted to this case. Nevertheless, the increasing flange of the in-phase function always corresponds to the heat-transfer mode, and the decreasing flange corresponds to the mass-transfer mode, and the heat- and mass-transfer kinetic parameters are still well separated.

6. Another important aspect of the frequency response technique is its capability of separating Fickian diffusion from surface barrier effects. Figure 6 shows the temperature characteristic functions for the two extreme cases when only one effect occurs. When the mass-transfer diffusion is dominant, the decreasing rate of the in-phase function and the amplitude of the minimum of the out-of-phase function are much smaller than in the case of dominant surface resistance.

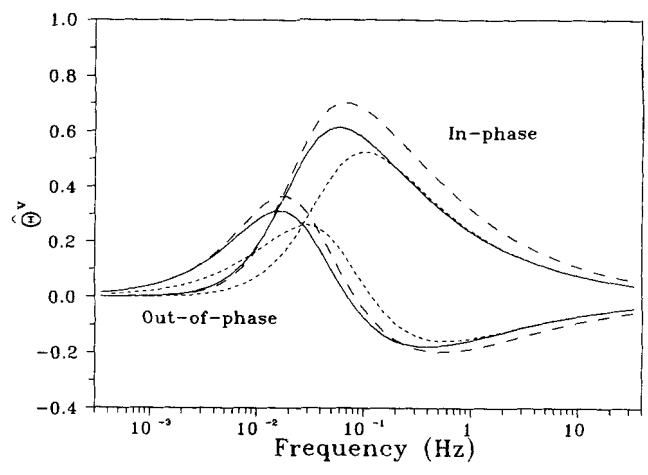

Figure 5. Calculated characteristic functions $\hat{\theta}_{in}^{v}$ and $\hat{\theta}_{out}^{v}$ for (——) $\tau_h = 10$ s, $\tau_{Dc} = 10$ s; (------) $\tau_h = 5$ s; $\tau_{Dc} = 10$ s; (---) $\tau_h = 10$ s, $\tau_{Dc} = 5$ s.

Experimental Setup

The experimental setup is described elsewhere (Grenier and Bourdin, 1994) and is presented in Figure 7. Its main features are as follows: The sample is placed in a chamber (~ 600 cm^3) with a bellows that can be moved sinusoidally at frequencies between 10^{-4} and 25 Hz. The pressure is recorded through a fast-response ($\tau = 1$ ms) Baratron gauge. The temperature is measured by IR detection. Let us recall the main advantages of the IR temperature measurement:

- *Very high response speed:* 1 ms of time constant for the whole detection chain is easily achieved.
- *Nonintrusive measurement:* Parasitic heat flux, thermal capacity of a sensor, and power dissipation are avoided.
- *Local measurement:* In most cases, the depth under the surface of the sample from which the IR emission is received does not exceed a few microns. As pointed out previously, this allows the separation of macropore and micropore diffusion in bidispersed samples and the identification of the bulk thermal conductivity.

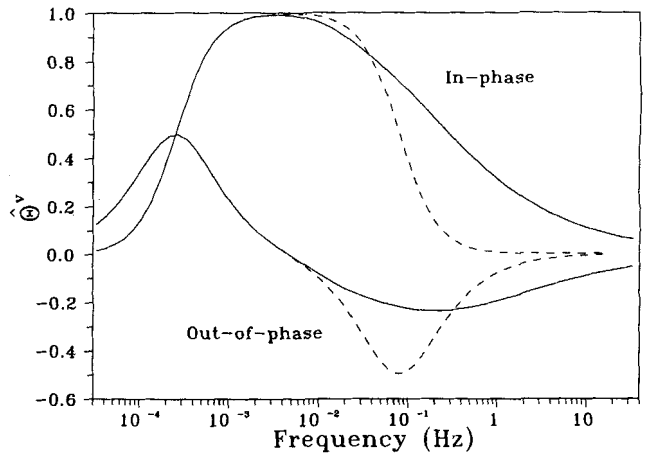

Figure 6. Calculated characteristic functions $\hat{\theta}_{in}^{v}$ and $\hat{\theta}_{out}^{v}$ for (——) $\tau_{Dp} = 0$ s, $\tau_{Dc} = 10$ s; (------) $\tau_{Dp} = 10$s, $\tau_{Dc} = 0$.

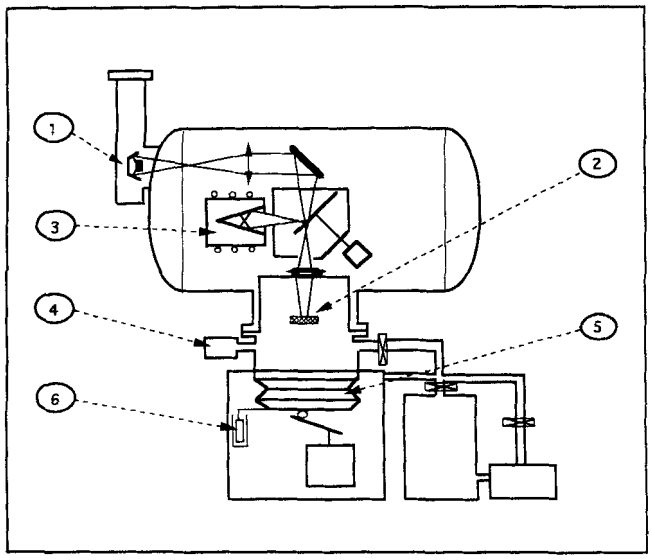

Figure 7. Experimental apparatus: (1) infrared detector; (2) sample; (3) controlled temperature black body; (4) pressure gauge; (5) bellows; (6) position gauge.

The stepper motor is run at a fixed speed to achieve a constant frequency volume variation. The volume, pressure, and temperature are recorded simultaneously (time slew artifact: 30 μs) at a sampling rate up to 10^3 per second, depending on the frequency. The duration of each record is fixed in order to obtain a minimum of three cycles for the lowest frequencies and a maximum of 10^4 sampling points (10 s) for the highest frequencies. The signal is numerically treated by the Fourier transform method in order to determine the amplitudes and phases of the pressure and temperature vs. frequency, taking the volume as reference. The amplitude and phase of the temperature, with the pressure as reference, are then determined following Eq. 10 to eliminate all spurious effects like adsorption on the walls of the experimental chamber or excess pressure amplitude due to nonisothermal compression.

The entire frequency domain is covered with approximately 30 fixed frequencies in geometrical progression.

Results

Some experimental results are presented here to illustrate the possibilities of the method. The main relevant parameters occurring in these experiments are summarized in Table 2. The parameters used to fit the experimental data are given in Table 3.

Blank experiments

Blank experiments performed on glass beads (0.5-mm diameter) permit the determination of the experimental uncertainty and the influence of the nonisothermal compression of the gas. The mean value of the temperature amplitude vs. the frequency obtained with carbon dioxide at 10^4 Pa is shown in Figure 8. The standard error is also plotted in the figure. It can be seen that the dispersion of the data is less than 10^{-4} K for $f < 0.1$ Hz and never exceeds 5×10^{-4} K. At high frequency the heat effect of the gas compression appears clearly, but remains reasonably small. This effect is proportional to the thermal mass of the gas, and thus to the pressure (Bourdin et al., submitted), and becomes completely negligible at pressures less than 1 kPa.

It appears that the minimum detectable concentration change for a system such as 5A-propane ($\Delta H \backsim 10^6$ J·kg^{-1} and $C_s \backsim 10^6$ J·m^{-3}·K^{-1}) is on the order of 10^{-4} kg·m^{-3}. This high sensitivity on the adsorbed amount measurement is not affected by the mass of the sample, which may be as small as few mg if pressure measurements are not needed.

NaX-water system

Crystals. Experiments have been performed on 100-μm NaX crystals provided by J. Kärger (Leipzig University) and synthesized in Zdhanov's laboratory. The mass of the sample was about 70 mg. Before experiments, the crystals were regenerated by heating under vacuum at 400°C overnight outside of the chamber, and heated *in situ* at a moderate temperature (250°C) under vacuum. Experiments at constant total mass of water were performed at various pressures and temperatures. Figure 9 shows the results obtained at 153 Pa and 25°C, and the experimental data are processed using the pressure as reference. It can be seen that the increasing flange of the in-phase function is well separated from the decreasing flange. This indicates that the thermal relaxation characteristic time is much greater than the mass transfer one. The corresponding kinetic parameters can be determined separately because they affect two different parts of the frequency range. One can see that good agreement with the model can be achieved.

On the other hand, it is not possible to obtain a good fit of the data when they are referenced to the volume. Figure 10 shows the same experimental data taking separately both the measured pressure and the volume as reference. The large difference observed may be attributed to the sorption of the water on the chamber walls, which would be responsible for the pressure not responding as expected to the volume modulation. When the pressure is taken as reference, the influence of the chamber walls is eliminated. In order to confirm this assumption, a blank experiment was performed without sam-

Table 2. Relevant Main Parameters of the Experiments

No.	System	Nature	σ	ν	Rc μm	Rp m	Pe Pa	Te K	C_s J·m^{-3}·K^{-1}	ΔH J·kg^{-1}	K_p kg·m^{-3}·Pa^{-1}	K_T kg·m^{-3}·K^{-1}	γ	K
1	NaX-H_2O	crystals	2		50		153	304	2.9×10^6	3.1×10^6	0.28	−3.23	3.7	2.9
2	NaX-H_2O	crystals	2		50		660	328	2.9×10^6	3.1×10^6	0.076	−3.22	3.8	0.3
3	NaX-H_2O	pellets	2	2	1.3	5×10^{-4}	97	298	3.1×10^6	3.1×10^6	0.435	−3.22	3.1	12
4	5A-C_3H_8	crystals	2		17		866	299	1.5×10^6	8.4×10^5	0.043	−1.86	0.25	1.2
5	5A-C_3H_8	pellets	2	1	1.2	8×10^{-4}	860	299	1.4×10^6	8.4×10^5	0.019	−0.86	0.5	1.8

Table 3. Kinetic Parameters Used in the Model to Fit the Experimental Data

Fig.	No.	D_c $m^2 \cdot s^{-1} \times 10^{12}$	k_c $m \cdot s^{-1} \times 10^{-6}$	D_p $m^2 \cdot s^{-1} \times 10^{-6}$	k_p $m \cdot s^{-1}$	h $W \cdot m^{-2} \cdot K^{-1}$	λ $W \cdot m^{-1} \cdot K^{-1}$	τ_{Dc} s	τ_{sc} s	τ_{Dp} s	τ_{sp} s	τ_h s	τ_λ s
9	1												
——		700	4,200			1.1		0.23	0.016			196	
------		500	4,200			1.1		0.32	0.016			196	
– – –		1,000	4,200			1.1		0.16	0.016			196	
12													
	1	700	4,200			1.1		0.23	0.016			196	
– – –	2	3,100	900			4.0		0.054	0.019			50.3	
13	2												
——		3,100	900			4.0		0.054	0.019			50.3	
– – –		3,100	650			4.0		0.054	0.026			50.3	
— —		3,100	1,300			4.0		0.054	0.013			50.3	
------		3,100	$\gg 1$			4.0		0.054	0			50.3	
14	3												
——		700	$\gg 1$	90	$\gg 1$	7.0	0.3	$<10^{-3}$	0	18	0	187	0.43
------		700	$\gg 1$	90	$\gg 1$	10.0	0.3	$<10^{-3}$	0	18	0	130	0.43
– – –		700	$\gg 1$	90	$\gg 1$	5.0	0.3	$<10^{-3}$	0	18	0	260	0.43
15	3												
——		700	$\gg 1$	90	$\gg 1$	7.0	0.3	$<10^{-3}$	0	18	0	187	0.43
------		700	$\gg 1$	130	$\gg 1$	7.0	0.3	$<10^{-3}$	0	12.5	0	187	0.43
– – –		700	$\gg 1$	65	$\gg 1$	7.0	0.3	$<10^{-3}$	0	25	0	187	0.43
16	3												
——		700	$\gg 1$	90	$\gg 1$	7.0	0.3	$<10^{-3}$	0	18	0	187	0.43
------		700	$\gg 1$	90	$\gg 1$	7.0	0.1	$<10^{-3}$	0	18	0	187	1.3
– – –		700	$\gg 1$	90	$\gg 1$	7.0	$\gg 1$	$<10^{-3}$	0	18	0	187	0
17	3												
——		10	$\gg 1$	90	$\gg 1$	7.0	0.3	0.011	0	18	0	187	0.43
------		3	$\gg 1$	90	$\gg 1$	7.0	0.3	0.038	0	18	0	187	0.43
– – –		1	$\gg 1$	90	$\gg 1$	7.0	0.3	0.11	0	18	0	187	0.43
18	4												
——		$\gg 1$	1.6			0.25		0	3.6			69	
------		20	2.2			0.25		1	2.6			69	
– – –		5.3	$\gg 1$			0.25		3.6	0			69	
19a	5												
——		$\gg 1$	1.6	10	0.035	3.5	0.24	0	0.018	14	20	145	0.7
------		$\gg 1$	1.6	4.2	$\gg 1$	3.5	0.24	0	0.018	34	0	145	0.7
– – –		$\gg 1$	1.6	$\gg 1$	0.021	3.5	0.24	0	0.018	0	34	145	0.7
19b	5	$\gg 1$	1.6	10	0.035	3.5	0.24	0	0.018	14	20	145	0.7

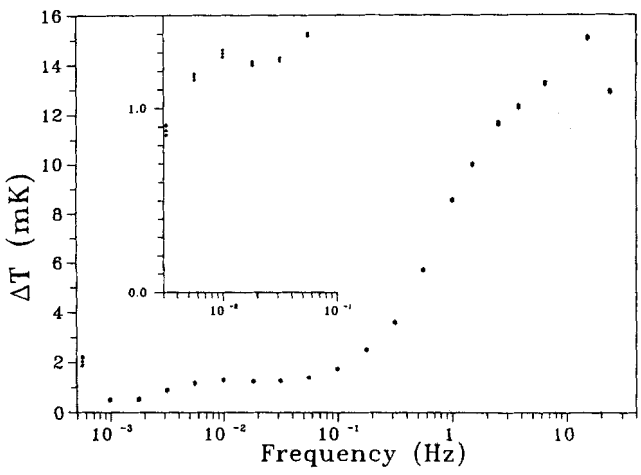

Figure 8. Blank experiment on glass beads 0.5 mm.

The standard error is calculated for each frequency. For $f <$ 0.1 Hz, the standard error is less than 10^{-4} K.

ple. Figure 11 shows clearly that the characteristic pressure functions are not zero as they would be in the absence of adsorption, and this confirms the influence of the chamber walls.

The diffusivity is determined with good precision even for such a fast diffusing system. Figure 9 shows that the experimental data are bracketed between the theoretical curves obtained for $D_c = 1 \times 10^{-9}$ and $D_c = 5 \times 10^{-10}$ $m^2 \cdot s^{-1}$. In this case, the Fickian diffusivity is dominant ($\tau_{Dc} = 230$ ms), and only a very small surface barrier ($\tau_{sc} = 16$ ms) is introduced to obtain the best agreement. The value $D_0 = 7 \times 10^{-11} m^2 \cdot s^{-1}$ is obtained after applying the Darken correction

$$D_0 = D_c [d \ln q / d \ln P]_T \tag{24}$$

to the best estimate of the diffusivity ($D_c = 7 \times 10^{-10} m^2 \cdot s^{-1}$). This value is close to the value obtained by nuclear magnetic resonance (NMR) ($D = 9 \times 10^{-11} m^2 \cdot s^{-1}$) (Pfeifer, 1976).

Measurements were also performed on the same sample at 660 Pa and 55°C. The experimental data and the best fit ref-

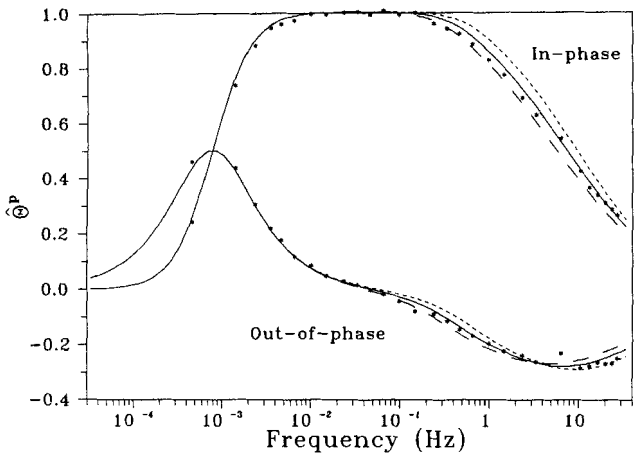

Figure 9. NaX-water: 73-mg 100-μm crystals at 153 Pa and 31°C (○○○○) measured $\hat{\theta}^p_{in}$ and (****) measured $\hat{\theta}^p_{out}$; Calculated functions for (——) $D_c = 7\times10^{-10}$ m$^2\cdot$s^{-1}, $\tau_{Dc} = 0.23$ s; (- - -) $D_c = 5\times10^{-10}$ m$^2\cdot$s^{-1}; (------) $D_c = 1\times10^{-9}$ m$^2\cdot$s^{-1}; ($k_c = 4.2\times10^{-3}$ m$\cdot$s^{-1}; $\tau_{sc} = 16\times10^{-3}$ s).

erenced to the pressure are plotted on Figure 12. The preceding results at lower temperature are also plotted in the figure for direct comparison: one can see that the curves at higher temperature are displaced toward the high frequencies. This indicates a faster overall kinetics. The values of the kinetic parameters that give the best fit are:

$$D_c = 3.1\times10^{-9}\text{m}^2\cdot\text{s}^{-1} \qquad (D_0 = 4\times10^{-10}\text{m}^2\cdot\text{s}^{-1})$$

$$\text{and} \qquad k_c = 9\times10^{-4}\text{m}\cdot\text{s}^{-1}.$$

Figure 13 shows the influence of a surface barrier on the temperature response. This figure shows the theoretical

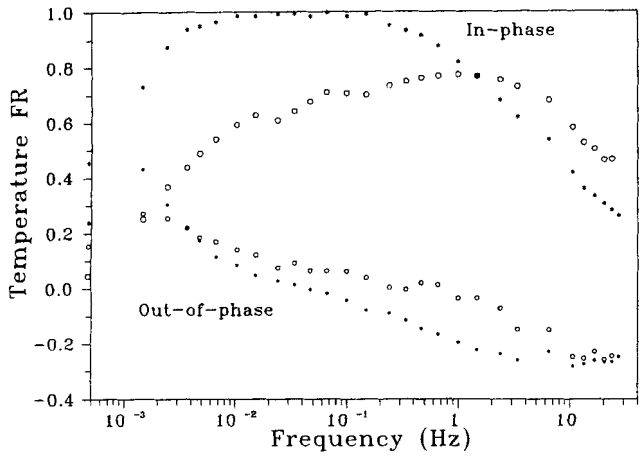

Figure 10. Experimental data on NaX-water system (73-mg 100-μm crystals at 153 Pa and 31°C): (○○○○) measured $\hat{\theta}^v_{in}$ and $\hat{\theta}^v_{out}$ (volume as reference): (****) measured $\hat{\theta}^p_{in}$ and $\hat{\theta}^p_{out}$ (measured pressure as reference).

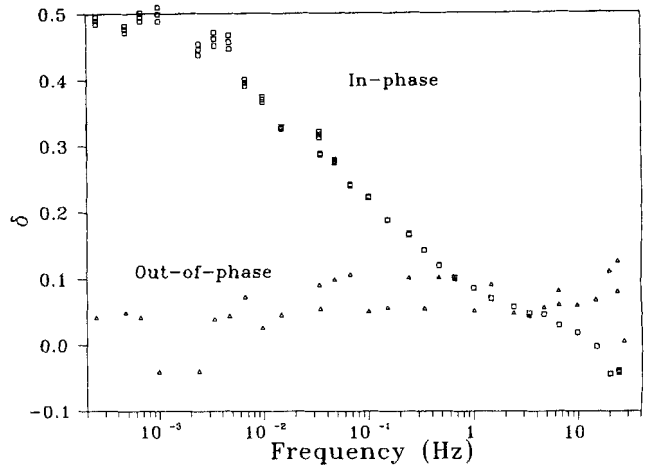

Figure 11. Experimental pressure functions δ_{in} and δ_{out} for a blank experiment (water without sample).

curves obtained with different values of the surfave barrier coefficient k_c. It can be seen that the introduction of a surface barrier ($6.5\times10^{-4} < k_c < 13\times10^{-4}$ m$\cdot$s^{-1}, 19 ms mean characteristic time) is necessary to obtain a good agreement at the higher frequencies. Nevertheless, the diffusion is dominant (54 ms characteristic time).

Pellets. Experiments were performed on 1-mm industrial NaX pellets (Siliporite G5, provided by CECA). These pellets are made of 2.6-μm-diameter crystals with a 20% clay binder. Since these pellets were preactivated, only a moderate *in-situ* activation at 250°C was performed.

The identification of the kinetic parameters is performed as follows: Starting from reasonable initial values for all parameters (surface barriers are not introduced at the beginning), the heat-transfer coefficient h is identified by adjusting the model to the experimental data in the low-frequency do-

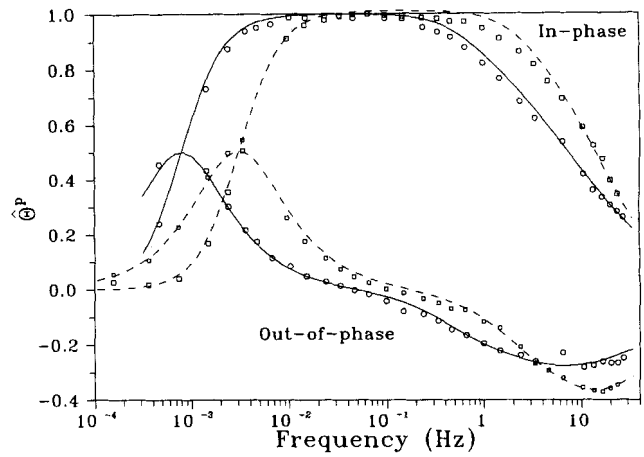

Figure 12. Na-X water: 73-mg 100-μm crystals: measured $\hat{\theta}^p_{in}$ and $\hat{\theta}^p_{out}$; (○○○○) 153 Pa and 31°C; (□□□□) 660 Pa and 55°C; (——) model with $D_c = 7\times10^{-10}$ m$^2\cdot$s^{-1} and $k_s = 4.2\times10^{-3}$ m$\cdot$s^{-1}; (- - -) model with $D_c = 3.1\times10^{-9}$ m$^2\cdot$s^{-1} and $k_s = 9\times10^{-4}$ m$\cdot$s^{-1}.

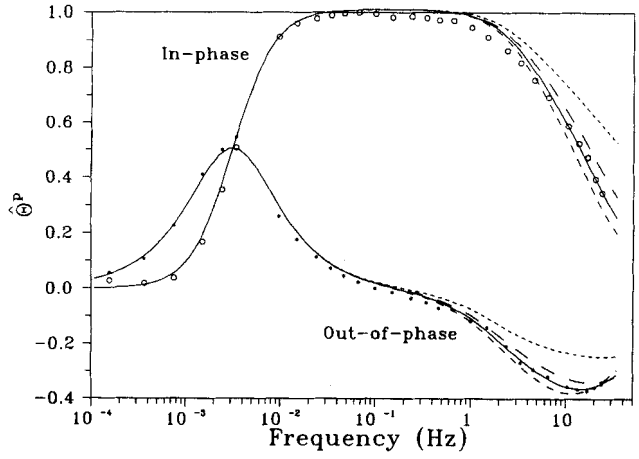

Figure 13. NaX-water: 73-mg 100-μm crystals at 660 Pa and 55°C: (○○○○) measured $\hat{\theta}_{in}^{p}$ and (****) measured $\hat{\theta}_{out}^{p}$; model with $D_c = 3.1\times10^{-9}$ m$^2\cdot$s^{-1} and (---) $k_c = 6.5\times10^{-4}$ m$\cdot$s^{-1}; (——) $k_c = 9\times10^{-4}$ m$\cdot$s^{-1}; (---) $k_c = 13\times10^{-4}$ m$\cdot$s^{-1}; and (------) $k_c \gg 1$.

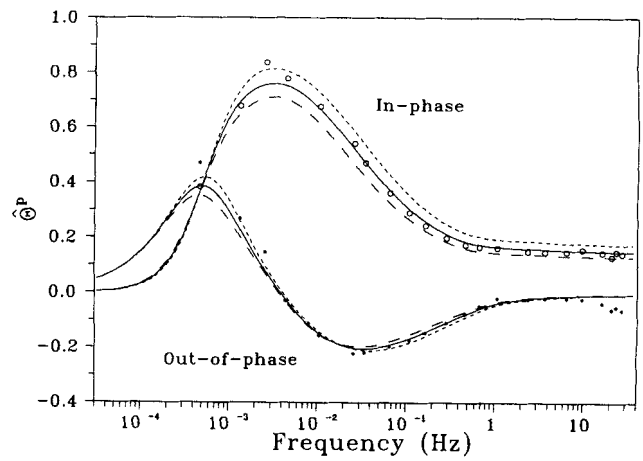

Figure 15. Na-X water: 0.8-g 1-mm pellets at 97 Pa and 25°C: (○○○○) measured $\hat{\theta}_{in}^{p}$ and (****) measured $\hat{\theta}_{out}^{p}$; model with (——) $D_p = 9\times10^{-5}$ m$^2\cdot$s^{-1}; (------) $D_p = 13\times10^{-5}$ m$^2\cdot$s^{-1}; and (---) $D_p = 6.5\times10^{-5}$ m$^2\cdot$s^{-1}.

main ($f < 2\times10^{-3}$ Hz). Figure 14 shows the identification of the coefficient h on the experimental results obtained at 97 Pa and 25°C: varying h keeps the high-frequency domain unaffected. The macropore diffusivity D_p is then identified using the decreasing side of the in-phase curve in the middle frequency range (0.01 to 0.1 Hz). It may be accurately determined, as seen on Figure 15. The identified value is $D_p = 9\times10^{-5}$ m$^2\cdot$s^{-1}. This value may be compared with the value $D_K = 1.5\times10^{-4}$m$^2\cdot$s^{-1} calculated from the Knudsen diffusion in straight channels with the mean diameter of the macropores (0.35 μm).

In the higher frequency domain ($f > 1$ Hz), the in-phase function keeps a constant value, depending on the macroporous diffusion coefficient D_p and the thermal conductivity λ. Figure 16 shows the influence of λ without modifying the previous identified value of D_p. The best identified value or λ is $\lambda \backsim 0.3$ W/m$\cdot$K. The value obtained is close to the value identified on 4-mm pellets using the pressure step method (Grenier et al., to be published) and by bed conductivity measurement (Sahnoune and Grenier, 1992).

Finally, despite the small size of the crystals, it is possible to assign a high minimum value to the microporous diffusivity from the experimental data on the pellets. Figure 17 shows that the in-phase experimental response remains constant for $f > 1$ Hz until the maximum measurable frequency ($\backsim$ 25 Hz). The corresponding response calculated for $D_c = 10^{-11}$ m$^2\cdot$s^{-1} decreases for $f > \backsim 4$ Hz. This allows us to conclude that $D_c > 10^{-11}$ m$^2\cdot$s^{-1}. The corresponding characteristic time is about 0.9 ms. This value represents approximately the measurement limit of the present experimental setup.

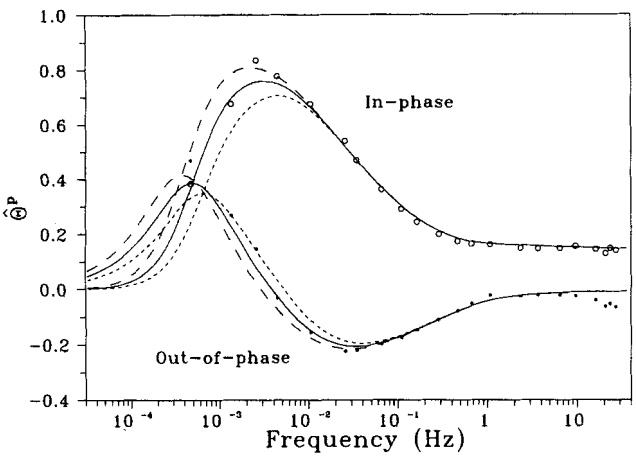

Figure 14. Na-X water: 0.8-g 1-mm pellets at 97 Pa and 25°C: (○○○○) measured $\hat{\theta}_{in}^{p}$ and (****) measured $\hat{\theta}_{out}^{p}$; model with (——) $h = 7$ W$\cdot$m$^{-2}\cdot$K^{-1}; (------) $h = 10$ W$\cdot$m$^{-2}\cdot$K^{-1}; and (---) $h = 5$ W$\cdot$m$^{-2}\cdot$K^{-1}.

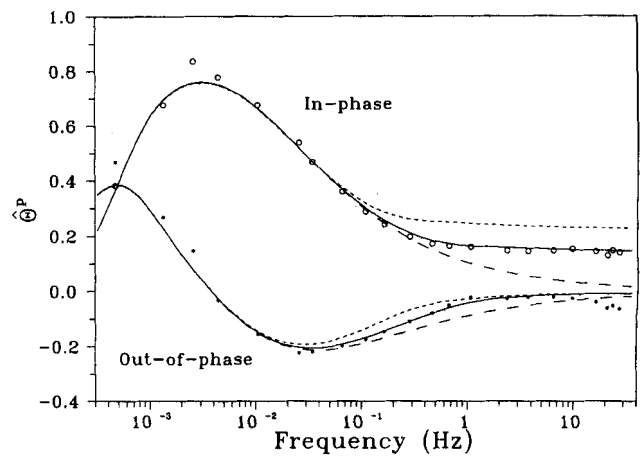

Figure 16. NaX-water: 0.8-g 1-mm pellets at 97 Pa and 25°C: (○○○○) measured $\hat{\theta}_{in}^{p}$ and (****) measured $\hat{\theta}_{out}^{p}$; model with (——) $\lambda = 0.3$ W$\cdot$m$^{-1}\cdot$K^{-1}; (------) $\lambda = 0.1$ W$\cdot$m$^{-1}\cdot$K^{-1}; and (---) $\lambda \gg 1$.

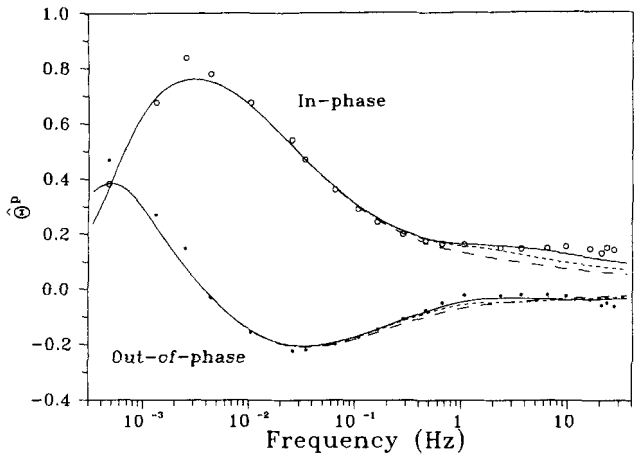

Figure 17. NaX-water: 0.8-g 1-mm pellets at 97 Pa and 25°C: (○○○○) measured $\hat{\theta}^P_{in}$ and (****) measured $\hat{\theta}^P_{out}$; model with (——) $D_c = 1\times10^{-11}$ $m^2\cdot s^{-1}$; (------) $D_c = 3\times10^{-12}$ $m^2\cdot s^{-1}$; and (---) $D_c = 1\times10^{-12}$ $m^2\cdot s^{-1}$.

5A-propane system

As with the NaX-water system, experiments have been performed on crystals and pellets. These samples, crystals as well as pellets, were heated *in situ* under vacuum at 400°C overnight. Unfortunately, metal deposits on the chamber walls were observed after the experiments were performed. These deposits were attributed to the overheating of soldered wires in the furnace placed inside the chamber. Most probably the sample was contaminated during activation. Nevertheless, the results are presented here since they are a good illustration of the discrimination between mass diffusion limitations and surface barrier effects. The results also demonstrate the information that can be extracted from experimental data.

Crystals. The crystals used for the experiments are 34-μm 5A crystals provided by D. M. Ruthven (University of New Brunswick). The mass of crystals was 435 mg. Figure 18 shows the characteristic experimental functions obtained for propane at 866 Pa and 26°C (the corresponding loading is 4.2 molecules per cage), as well as the characteristic functions calculated with the model. Since a pure diffusion model cannot fit the experimental data (large dotted lines), a surface barrier was introduced to run the model. As can be seen, the best fit is obtained with a pure surface barrier with a characteristic time of 3.6 s ($k_c = 1.6\times10^{-6}$ $m\cdot s^{-1}$). The lower limit of the diffusivity estimated from the present measurements is about 2×10^{-11} $m^2\cdot s^{-1}$ ($\tau_{Dc} < 1$ s) (small dotted lines). This value is much larger than the value extrapolated to 300 K from the results obtained by NMR for a loading of 3.5 molecules per cage (Kärger and Ruthven, 1981), which is about $D_s = 10^{-12}$ $m^2\cdot s^{-1}$. If the surface barrier was misinterpreted as an internal diffusion process, its characteristic time of 3.6 s would correspond to an uncorrected diffusivity of 5×10^{-12} $m^2\cdot s^{-1}$, which remains larger than the value given by NMR. The presence of a dominant surface barrier can be explained by the contamination of the crystals in the chamber during the reactivation, as pointed out previously, but this explanation does not account for the high lower limit of the diffusivity. Some further measurements are necessary to clarify the exact origin of the surface barrier observed experimentally and the high internal diffusivity as compared to NMR measurements.

Pellets. The experiments reported here were performed on 1.6-mm-diameter cylindrical industrial pellets provided by Rhône Poulenc. As for NaX pellets, the 5A 2.4-μm crystals are agglomerated with 20% of clay. The results for a pellet monolayer (1.8 g) sample with propane at 860 Pa and 26°C are given on Figure 19a. Experimental results are compared to three theoretical simulations: the long dots correspond to a nonisothermal bidispersed case, where the crystal kinetics was equal to the one obtained from the previous results, and a purely diffusive model, which was taken for the mass transport properties in the macropores. Obviously, the numerical results do not at all match our experimental results. The solid line was obtained using the same kinetics for the crystals, but assuming a surface barrier at the pellet surface ($k_p = 3.5\times10^{-2}$ $m\cdot s^{-1}$, $\tau_{sp} = 20$ s), and an excellent fit was obtained. The third curve (short dots) was obtained by assuming that the kinetics was completely controlled at the crystal level. It would be necessary, in this case, to take $D_c = 5\times10^{-15}$ $m^2\cdot s^{-1}$ and $k_c = 2.8\times10^{-8}$ $m\cdot s^{-1}$. The numerical results are close to the experimental results but this solution is rejected, since it does not correspond at all to what has been measured on the crystals.

It has to be noted that in the case of a contaminated sample it is not possible to extract from a single sample all the kinetic data, as it was for the case of NaX-water, because the characteristic time of a surface barrier at the macroporous level is greater than the time of the heat diffusion in the pellet. The surface temperature is nothing but the mean temperature of the pellet, and it gives no information about the mass transfer at the microporous level. In this case, it is not possible to clearly separate the influences of the macro- and microporous mass-transfer kinetics because either a macro-

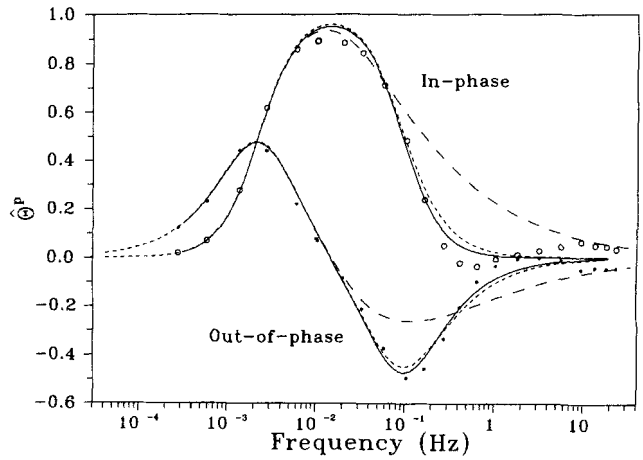

Figure 18. 5A-propane: 0.5-g 34-μm crystals at 866 Pa and 25°C: (○○○○) measured $\hat{\theta}^P_{in}$ and (****) measured $\hat{\theta}^P_{out}$; (——) model with pure surface barrier ($k_c = 1.6\times10^{-6}$ $m\cdot s^{-1}$); (---) model with pure diffusion ($D_c = 5.3\times10^{-12}$ $m^2\cdot s^{-1}$); (------) model with $D_c = 2\times10^{-11}$ $m^2\cdot s^{-1}$ and $k_c = 2.2\times10^{-6}$ $m\cdot s^{-1}$ (mass-transfer characteristic time in all cases: 3.6 s).

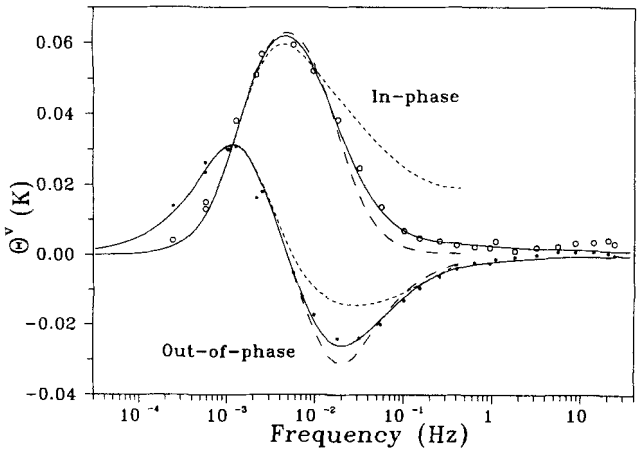

(a)

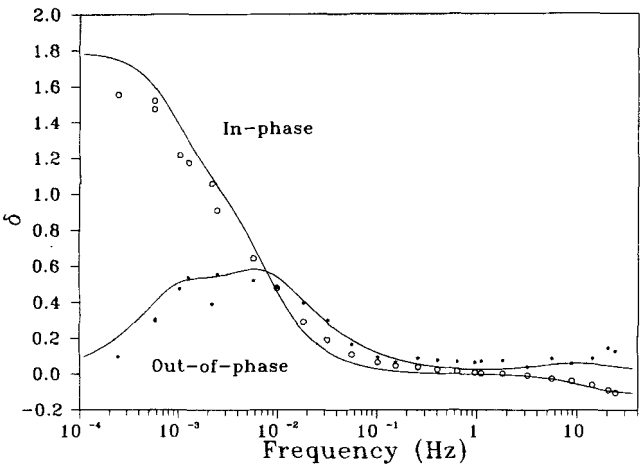

(b)

Figure 19. (a) 5A-propane: 1.8-g 1.6-mm pellets at 890 Pa and 26°C: (○○○○) measured $\hat{\theta}_{in}^{v}$ and (****) measured $\hat{\theta}_{out}^{v}$ (not normalized); (——) model with $D_p = 1.0\times10^{-5}$ m$^2\cdot$s^{-1} and $k_p = 3.5\times10^{-2}$ m$\cdot$s^{-1}; (------) model with $D_p = 4.2\times10^{-6}$ m$^2\cdot$s^{-1} and $k_p \gg 1$; (– – –) model with $D_p \gg 1$ and $k_p = 2.1\times10^{-2}$ m$\cdot$s^{-1}: (b) 5A-propane: 1.8-g 1.6-mm pellets at 890 Pa and 26°C: (○○○○) measured δ_{in}; (****) measured δ_{out}; (——) model with $D_p = 1.0\times10^{-5}$ m$^2\cdot$s^{-1} and $k_p = 3.5\times10^{-2}$ m$\cdot$s^{-1}.

porous surface barrier hides the microporous transfer, or the microporous transfer is much slower than the heat diffusion in the pellet and its surface temperature is the same as its mean temperature.

This sample is large enough to obtain a good pressure response. Figure 19b shows the in- and out-of-phase experimental curves for the pressure and the curves calculated with the macroporous kinetic parameters identified from the temperature response taking the volume as reference. The good agreement with the experimental data indicates that with propane, the influence of the chamber wall adsorption is small.

A new design of the oven outside of the chamber is currently being carried out and will avoid any contamination in the future. Some further measurements will be performed with the new design to clarify the origin of the surface barriers.

Conclusion

The thermal frequency response method using IR detection to measure the temperature of the sample appears to be a powerful method for determining adsorption kinetics parameters in adsorbents, especially in mono- or bidispersed samples of zeolite. The high-temperature sensitivity of the IR detection allows the measurement of the quasi totality of the zeolitic adsorbent–adsorbate systems. The technique discussed herein presents the same advantages as the frequency response technique that measures only the pressure. It distinguishes between the different physical modes that limit the kinetics: thermal transfer in- and outside the pellets; two-scale Fickian diffusion; and surface barrier. These different rate-limiting modes are easily distinguished if their characteristic times are different, especially when the thermal relaxation characteristic time is large. In this later case, the influence of each rate-limiting effect on the experimental signal is reduced to a frequency window corresponding to its characteristic time. Moreover the very low overall measurement time constant ($\backsim$ 1 ms) allows the determination of fast kinetic parameters, up to $D_c = 10^{-7}$ m$^2\cdot$s^{-1} for 100-μm crystals, and permits us to obtain results comparable with the results given by microscopic methods.

An important improvement appears when both temperature and pressure measurements are performed. When the temperature amplitude and phase are expressed using the pressure amplitude and phase as references, the in- and out-of-phase functions depend only on the physical properties of the sample. All spurious influences are eliminated.

Moreover, for bidispersed sample, in the frequent cases where microporous kinetics is very fast owing to the smallness of the crystals, it is possible to determine separately the macroporous and the microporous kinetic parameters with a single size of pellets. This possibility is due to the finite heat diffusion in the pellet and to the ability of IR detection to measure precisely its surface temperature. Such a possibility does not exist when only the pressure is measured in a frequency response experiments.

Acknowledgment

We are grateful for financial support provided by the European Community under Joule Program (CEE JOU2-CT 92-0076).

Notation

C_s = total volumetric heat capacity of the sample, J$\cdot$m$^{-3}\cdot$K^{-1}
c_e = sorbate concentration in the macropores at equilibrium, kg$\cdot$m^{-3}
D_0 = corrected microporous diffusivity, m$^2\cdot$s^{-1}
K = adsorptive capacity coefficient: $\alpha(1+\beta)$ (Bidispersed case)
K_p = concentration derivative with respect to pressure, kg$\cdot$m$^{-3}\cdot$Pa^{-1}
K_T = concentration derivative with respect to temperature for crystal, kg$\cdot$m$^{-3}\cdot$K^{-1}
P_e = pressure for $V = V_e$ and $T = T_e$
p = relative amplitude of pressure variation
q = concentration of the sorbate, kg$\cdot$m^{-3}

q_e = concentration of the sorbate at equilibrium for $T = T_e$ and $P = P_e$, $kg \cdot m^{-3}$
R_e = heat capacity of the (ideal) gas, $J \cdot kg^{-1} \cdot K^{-1}$
R_c, R_p = radius of the crystals and the pellets, respectively, m
r_c, r_p = radial coordinate for crystals and pellets, respectively
t = time, s
V_g = experimental volume mean value, m^3
δ = normalized characteristic pressure function
ΔH = enthalpy of sorption, $J \cdot kg^{-1}$

Literature Cited

Bétemps, M., M. Mange, S. Scavarda, and A. Jutard, "Problèmes Posés par l'Application des Méthodes Classiques d'Identification des Processus à la Détermination du Coefficient de Diffusion des Gaz dans les Tamis Moléculaires," *J. Phys. D: Appl. Phys.*, **10**, 697 (1977).

Bourdin, V., L. M. Sun, Ph. Grenier, and F. Meunier, "Analysis of the Temperature Frequency Response for Diffusion in Crystals and Biporous Pellets," in press (1996).

Evnochides, S. K., and E. J. Henley, "Simultaneous Measurement of Vapor Diffusion and Solubility Coefficients in Polymers by Frequency Response Techniques," *J. Polymer Sci.*, **8**, 1987 (1970).

Grenier, Ph., V. Bourdin, L. M. Sun, and F. Meunier, "A Single Step Thermal Method to Measure Intracrystalline Mass Diffusion in Adsorbents," *AIChE J.*, **41**, 2047 (1995).

Grenier, Ph., and V. Bourdin, "Méthode Thermique d'Étude de la Cinétique d'Adsorption dans les Solides Microporeux," Congress of the "Société Française des Thermiciens," Paris (May 17–19, 1994).

Jordi, R. G., and D. D. Do, "Frequency-Response Analysis of Sorption in Zeolite Crystals with Finite Intracrystal Reversible Mass Exchange," *J. Chem. Soc., Farad. Trans.*, **88**(16), 2411 (1992).

Kärger, J., and D. M. Ruthven, "Diffusion in Zeolites. Comparison of Sorption and Nuclear Magnetic Resonance Diffusivities," *J. Chem. Soc., Farad. Trans.*, **77**(1), 1485 (1981).

Pfeifer, H., "Surface Phenomena Investigated by Nuclear Magnetic Resonance," *Phys. Rep. (Phys. Let., Sec. C.)*, **26**(7), 293 (1976).

Polinski, L. M., and L. M. Naphtali, "Dynamic Methods for Characterization of Adsorptive Properties of Solid Catalysts," *Adv. Catal.*, **19**, 241 (1963).

Sahnoune, H., and Ph. Grenier, "Mesure de la Conductivité Thermique d'une Zéolithe," *Chem. Eng. J.*, **40**, 45 (1989).

Sun, L. M., F. Meunier, and J. Kärger, "On the Heat Effect in Measurements of Sorption Kinetics by the Frequency Response Method," *Chem. Eng. Sci.*, **48**(4), 715 (1993).

Sun, L. M., and V. Bourdin, "Measurement of Intracrystalline Diffusion by the Frequency Response Method: Analysis and Interpretation of Bimodal Response Curves," *Chem. Eng. Sci.*, **48**(22), 3783 (1993).

Sun, L. M., F. Meunier, Ph. Grenier, and D. M. Ruthven, "Frequency Response for Nonisothermal Adsorption in Biporous Pellets," *Chem. Eng. Sci.*, **49**(3), 373 (1994).

Torresan, A., and Ph. Grenier, "Un Appareil pour la Mesure Thermique de la Cinétique d'Adsorption," *Chem. Eng. J.*, **49**, 11 (1992).

Van-Den-Begin, N. G., and L. V. C. Rees, "Diffusion of Hydrocarbons in Silicalite using Frequency-Response Method," *Zeolites: Facts, Figures, Future*, Elsevier, New York, p. 915 (1989).

Yasuda, Y., "Frequency Response Method for Study of the Kinetic Behavior of a Gas-Surface System," *J. Phys. Chem.*, **80**(17), 1867 (1976).

Yasuda, Y., "Frequency Response Method for Investigation of Gas-Surface Dynamic Phenomena," *Heterogeneous Chem. Rev.*, **1**, 1 (1994).

Zhong, G. M., Ph. Grenier, and F. Meunier, "Influence des Transferts Intergranulaires sur la Détermination de la Cinétique d'Adsorption," *Chem. Eng. J.*, **53**, 147 (1993).

Manuscript received Jan. 24, 1995, and revision received Apr. 26, 1995.